IOP Publishing Phys. Med. Biol. 65 (2020) 055010 (17pp) https://doi.org/10.1088/1361-6560/ab6b43

Physics in Medicine & Biology

IPEM Institute of Physics and Engineering in Medicine

PAPER

Heuristic tree searching for pose-independent 3D/2D rigid registration of vessel structures

RECEIVED
7 August 2019

REVISED
24 December 2019

ACCEPTED FOR PUBLICATION
14 January 2020

PUBLISHED
6 March 2020

Jianjun Zhu[1], Jingfan Fan[1], Shuai Guo[1], Danni Ai[1], Hong Song[2], Cheng Wang[3], Shoujun Zhou[3] and Jian Yang[1]

[1] Beijing Engineering Research Center of Mixed Reality and Advanced Display, School of Optics and Photonics, Beijing Institute of Technology, Beijing 100081, People's Republic of China
[2] School of Computer Science and Technology, Beijing Institute of Technology, Beijing 100081, People's Republic of China
[3] Shenzhen Institutes of Advanced Technology, Chinese Academy of Sciences, Shenzhen 518055, People's Republic of China

E-mail: jyang@bit.edu.cn

Keywords: 3D/2D registration, vessel graph matching, search tree

Abstract

The 3D/2D registration of pre-operative computed tomography angiography (CTA) and intra-operative x-ray angiography (XRA) images in vascular intervention is imperative for guiding surgical instruments and reducing the dosage of toxic contrast agents. In this study, 3D/2D vascular registration is formulated as a search tree problem on the basis of the topological continuity of vessels and the fact that matching can be decomposed into continuous states. In each node of the tree, a closed-solution of 3D/2D transformation is used to obtain the registration results based on the dense correspondences of vessel points, and the results of matching and registration are calculated and recorded. Then, a hand-crafted score that quantifies the qualities of matching and registration of vessels is used, and the remaining problem focuses on finding the highest score in the search tree. An improved heuristic tree search strategy is also proposed to find the best registration. The proposed method is evaluated and compared with four state-of-the-art methods. Experiments on simulated data demonstrate that our method is insensitive to initial pose and robust to noise and deformation. It outperforms other methods in terms of registering real model data and clinical coronary data. In the 3D/2D registration of uninitialized and initialized coronary arteries, the average registration errors are 1.85 and 1.79 mm, respectively. Given that the proposed method is independent of the initial pose, it can be used to navigate vascular intervention for clinical practice.

1. Introduction

At present, minimally invasive intervention is the main treatment for vascular pathology, and the operation of surgical instruments is guided by x-ray angiography (XRA) images during intervention. This image modality has satisfactory performance on the display of vessels lumen after a contrast agent is injected in the arteries of interest through a catheter. The surgical instruments that navigate inside the vasculature can also be displayed clearly in XRA. However, performing interventional operations accurately under the guidance of single-view 2D projection is difficult for interventional radiologists because of the absence of spatial information in XRA. Therefore, in interventional surgery, multi-view angiography images obtained by a rotating C-arm are used frequently, and the increasing dosage of toxic contrast agents can impose a burden on patients. To address this issue, a pre-operative computed tomography angiography (CTA) image can be used in combination with intraoperative XRA imaging. In this technique, the interventional image is augmented by projecting 3D vessels overlaid on 2D live images. Physicians and patients benefit from visualizing these different imaging modalities in one view. To achieve this goal, 3D/2D registration technology is mandatory for obtaining good alignment and relevant correspondences.

3D/2D registration methods use one 3D pre-interventional image and one or more intra-interventional 2D X-ray projection images as sources to perform the registration task (Markelj *et al* 2012). To establish 3D/2D registration, 3D and 2D image data as well as the C-arm geometry need to be required. For the x-ray image

Table 1 Overview of related works for 3D/2D registration.

Method/citation	Assumption	Basic work	Evaluation Metric	Application
ICP (Besl and McKay 1992, Baka *et al* 2014)	The closest relation determines correspondences of vessel points	Besl and McKay (1992)	Mean projection distance error	Coronary artery
Rivest-Henault *et al* (2012)		—	Mean projection distance error	Coronary artery
Benseghir *et al* (2013)	The closest relation determines correspondences of vessel curves	—	Mean projection distance error	Coronary artery
Kang *et al* (2013)	Assign probabilistic correspondences of vessel points by GMM	Myronenko and Song (2010)	Rotation and translation errors	Femoroplasty
Baka *et al* (2014)	The *L2* distance of two orientated GMM responses determines registration	Jian and Vemuri (2011)	Mean projection distance error, Success rate	Coronary artery
Benseghir *et al* (2015)	Tree topology preserves in the pairing procedure	Benseghir *et al* (2013)	Alignment and pairing errors	Coronary artery
Liu *et al* (2017)	Topology consistency crosses modalities	—	Mean projection distance error	Coronary artery
Varnavas *et al* (2015)	The initialization is based on preoperative computation of 2D templates over a wide range of 3D poses	—	True/false positive/negative rate	Lumbar spine
Miao *et al* (2013)	It establishes a shape context-encoded library of 2D contours and performed library matching.	—	*X*, *Y*, *Z* and angular differences, RMSD, Success rate	Metal implants
Gouveia *et al* (2017)	It relates the features of 2D projection images to rigid transformation parameters.	—	3D mean target registration error	Coronary artery

sequence, the 3D/2D registration is usually deemed to be 3D/2D + *t*. Rotational imaging is frequently used in clinical practice, which can produce multi-plane x-ray images. In that case, the multi-plane 3D/2D registration can be regarded as 3D/2.5D. Since the 3D/2D registration is the basis of the 3D/2D + *t* and the 3D/2.5D, only the registration from 3D image to one-frame mono-plane 2D image is discussed in this work. The 3D/2D registration methods can be classified into two classes according to the properties of the registration technique, namely, intensity- and feature-based methods. Intensity-based methods are generally conducted by optimizing the similarity measure between the projection of 3D pre-interventional image and 2D intra-interventional image. Digitally reconstructed radiography (DRR) (Dorgham *et al* 2012) and maximum intensity projection (MIP) (Kerrien *et al* 1999) are two common methods that generate simulated x-ray projections of a computed tomography (CT) image. Hipwell *et al* (2003) analyzed six similarity metrics between DRR/MIP and x-ray images, in which pattern intensity and gradient difference exhibit the best performance. Given that the intensity-based methods use the entire intensity information for registration, they are sensitive to background outliers. Furthermore, the optimizing-based method may produce a small capture range when aligning data with large-scale transformations.

Feature-based 3D/2D registration relies on consistent features that can be extracted from two modalities. The centerline is the most popular representation of features for vessel registration. Related feature-based methods are summarized in Table 1, including the applied assumption, the basic work, evaluation metric and clinical application. Iterative closest point (ICP) method (Besl and McKay 1992) uses a strategy in which registration can be regarded as a sequential alternating procedure that includes matching and registration phases. For the matching phase, point correspondence is assigned by searching for the minimal Euclidean distance of points. An extension of ICP for 3D/2D registration by back-projecting 2D points onto 3D space and then performing general ICP was introduced in Baka *et al* (2014). (Rivest-Henault *et al* 2012) used a precomputed distance transform of vessel centerline to construct the objective function, which could accelerate the registration procedure. Benseghir *et al* (2013) proposed the iterative closest curve (ICC) method, which uses the vessel branch as the elements for pairing based on the closest relation and then estimates the transformation that minimizes the sum of distances between the paired branches. These ICP-like methods are sensitive to noise and outliers because they restrict the correspondence to a one-to-one assignment. The closest relation-based pairing also causes these methods to rely heavily on the initial pose.

In a probabilistic assignment framework, soft assignment relaxes the one-to-one correspondence to one-to-many according to the sensitivity of hard assignment to noise and outliers. On the basis of the Gaussian mixture

model (GMM) and the expectation-maximization (EM) algorithm, (Myronenko and Song 2010) proposed the coherent point drift (CPD) method that forces GMM centroids to move coherently to preserve the global topological structure of point sets. Kang *et al* (2013) used the same framework as CPD for 3D/2D point set registration. When considering the nonlinear nature of perspective projections, particle swarm optimization (PSO) is used to solve the optimal estimation of the registration parameter in the maximization step. Baka *et al* (2014) proposed the oriented GMM (OGMM) method extended from (Jian and Vemuri 2011), it estimates the L_2 distance of two point sets with orientational information and optimizes it to achieve 3D/2D coronary artery registration. Given that the OGMM takes advantage of the orientation of the centerline, it can achieve high accuracy and robustness for noisy data.

With vessel topology being an invariant property across modalities and dimensions, graph matching becomes an effective vascular registration approach. In the literature, the matching of vessel graph has been described as starting to estimate correspondences of vessel bifurcations and then matching vessel curves between paired bifurcations by considering them as vertices. Serradell *et al* (2014) treated vessel registration as a searching process for most likely correspondences, and a priority search was conducted to accelerate the process. Pinheiro *et al* (2016) formulated vessel matching as a tree searching method on the basis of the topology consistency of two graphs to be matched, and the Monte Carlo tree search was applied to solve this problem. Moriconi *et al* (2018) defined a compatibility function of graph matching by setting node and edge attributes and then maximized the function of the quadratic assignment problem to obtain node pairing. These methods (Serradell *et al* 2014, Pinheiro *et al* 2016, Moriconi *et al* 2018) are all associated with 3D/3D or 2D/2D vasculature matching/registration. For 3D/2D vessel matching, the overlaps in projection determined that the outliers and noise should be emphasized in the method. The ICC method (Benseghir *et al* 2013) uses vessel topology by pairing curves between two nodes. For the noisy 2D graph, neighborhood relation is used to restrict admissible candidates. Benseghir *et al* (2015) proposed matching tree centerlines in a divide-and-conquer framework based on the ICC framework while ensuring the connectivity of bifurcation points. Liu *et al* (2017) regarded 3D and 2D vessels as tree topology and represented tree topology as a sequence; then, the vessel matching of nodes was achieved by performing sequence-to-sequence matching. The sequence was extracted using a topological sort algorithm by keeping the anteroposterior relationship, and then traversed in a successive order.

Optimization-based transformation calculation may also fall into the local extremum easily for the nonlinear nature of perspective projections, making these methods sensitive to the initial pose of registration. Initialization is crucial for 3D/2D registration. In general, pre-operative and intra-operative images are acquired from different equipment. The capture ranges of most registration methods are insufficient to recover the transformation between the coordinate systems of two acquisition modalities. Some initialization approaches, such as the alignment of patient position and orientation, the registration of corresponding pairs of markers, and the manual initialization were introduced in Markelj *et al* (2012). However, an automatic initialization method that uses intrinsic features is suitable for intraoperative 3D/2D registration. Varnavas *et al* (2015) precomputed 2D projection templates over a wide range of 3D poses and used the intra-operative image to evaluate the similarity between the templates and the Generalized Hough Transform of 2D fluoroscopy to obtain initial alignment. Miao *et al* (2013) established a shape context-encoded library of 2D contours extracted from the silhouettes of metal implants and adopted Jensen–Shannon divergence as the matching metric for fast library matching. Gouveia *et al* (2017) proposed a regression-based initial registration method of CTA and XRA that relates the features of 2D projection images to rigid transformation parameters.

For large capture range or non-sensitivity to the initial pose, the registration based on a match-then-transform framework (Fan *et al* 2016a, 2016b) is more appropriate than optimization-based methods. Given the correspondences of 3D and 2D points, the goal of 3D/2D registration is similar to the perspective-*n*-points (P*n*P) problem (Lepetit *et al* 2008) in the computer vision area. It aims to determine the camera pose by reducing the problem of estimating the transformation of paired points to that of estimating coordinates of four control points.

This work uses the topology consistency of 3D and 2D vessels to achieve vessel matching. The matching of two graphs can be formulated as a set of edge pairs in 3D and 2D. According to the topological continuity of vessel centerline, vessel matching can be regarded as a successive procedure of new paired edges being added to existing pairings. This property can decompose the matching procedure into successive states for search tree construction. In this work, our aim is to find the best state associated with optimal registration and matching in the search tree. We demonstrate the accuracy of our method by using simulated data, aorta model data, and clinical coronary arteries. The contributions of this work are twofold. First, the 3D/2D registration of vessel graphs is formulated as a tree-searching problem. At each node of the tree, a closed solution is used to calculate the registration result based on the dense matching of vessel points, and a node score that evaluates the qualities of matching and registration is designed. Second, on the basis of the A-star search algorithms, an improved heuristic tree search strategy is proposed to find the optimal result with the highest node score.

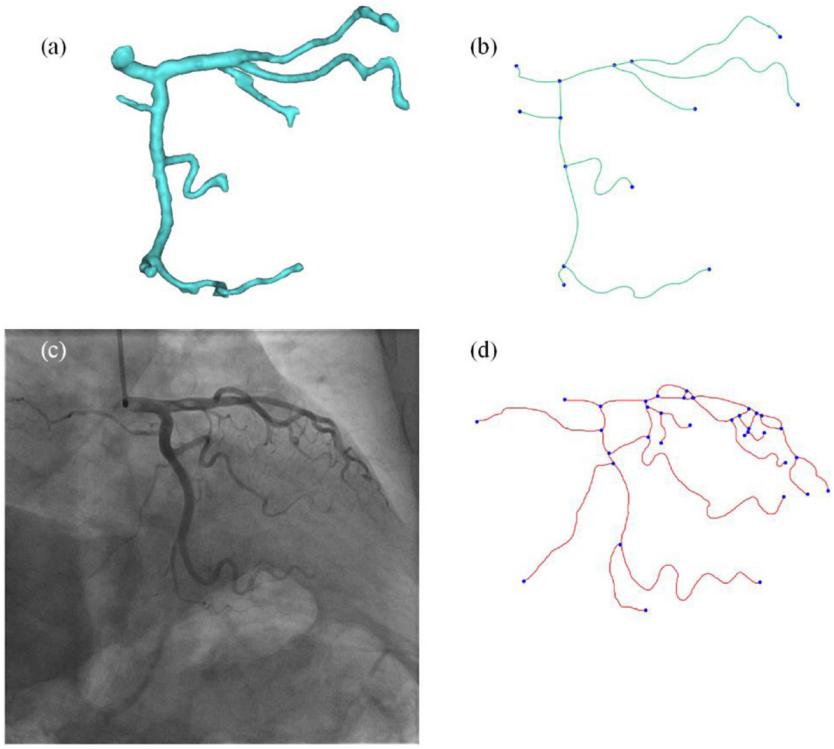

Figure 1. 3D and 2D vessels to be registered. (a) 3D vessel model; (b) 3D centerlines of (a); (c) 2D angiogram image; (d) 2D centerlines of (c). The blue points in (b) and (d) are vertices of graph and the curves that connect two incident vertices are edges of the graph.

2. Methods

2.1. Problem definition

A graph $\mathcal{G} = \{\mathcal{V}, \mathcal{E}\}$ in 3D or 2D can be constructed by the set of vertices $\mathcal{V}$ and set of edges $\mathcal{E}$. Set of vertices $\mathcal{V}$ includes the bifurcations and endpoints, shown as blue points in figures 1(b) and (d). Edge set $\mathcal{E}$ is associated with the curves that connect two incident vertices. The matching between 3D graph $\mathcal{G}^{3D} = \{\mathcal{V}^{3D}, \mathcal{E}^{3D}\}$ and 2D graph $\mathcal{G}^{2D} = \{\mathcal{V}^{2D}, \mathcal{E}^{2D}\}$ is strongly reliant on an assumption that a vertex $v_i^{3D} \in \mathcal{V}^{3D}$ in 3D corresponds to a vertex $v_j^{2D} \in \mathcal{V}^{2D}$ in 2D and that an edge $e_i^{3D} \in \mathcal{E}^{3D}$ of the 3D graph should be matched with an edge $e_j^{2D} \in \mathcal{E}^{2D}$ of the 2D graph. The matching of two graphs $\mathcal{G}^{3D}$ and $\mathcal{G}^{2D}$ can be represted as sets of vertex pair $\pi^{\mathcal{V}} = \left\{\left(v_i^{3D}, v_j^{2D}\right)\right\}$ and edge pair $\pi^{\mathcal{E}} = \left\{\left(e_i^{3D}, e_j^{2D}\right)\right\}$. Given that the end-vertices of matched edges are matched and no other vertices are involved, edge matching $\pi^{\mathcal{E}}$ uniquely determines a vertex matching $\pi^{\mathcal{V}}$.

In this study, a 3D vessel is considered an acyclic graph, while a 2D vessel is generally represented by a cyclic 2D graph because several projected 3D branches will overlap in the 2D plane, thus forming fake bifurcations and connecting edges. Furthermore, because contrast agents are injected globally in CTA and locally through a catheter in XRA (Groher *et al* 2007), as well as the segmentation error and noise, 3D and 2D vessel graphs are distinctly different (figure 1). The topological differences between 3D and 2D graphs will hinder the matching. To address this issue in this work, the superedges (Pinheiro *et al* 2016), which are defined as sequences of multiple consecutive edges, are applied. In the definition, the superedge set contains a regular edge set, and we still use $\mathcal{E}$ to denote the superedge set.

The registration of 3D and 2D vessel structures can be formulated as finding an optimal transformation T of the 3D vessel whose projection best aligns the 2D vessel,

$$\widehat{T} = \underset{T}{\operatorname{argmin}}\, \mathcal{D}\left(P \circ T\left(\mathcal{G}^{3D}\right), \mathcal{G}^{2D}\right), \tag{1}$$

where T indicates a set of admissible transformation, and $\mathcal{D}$ quantifies the distance between two graphs or two edges. P denotes a perspective projection operation that is constant and mandatory to compare a 3D and 2D modality and can be established using several parameters obtained from the DICOM head file of XRA. With the matching $\pi^{\mathcal{E}} = \left\{\left(e_i^{3D}, e_j^{2D}\right)\right\}$ of two graphs consisting of all matched superedges, the registration can be reformulated as finding an optimal transformation of the 3D vessel such that each 3D superedge best aligns with the 2D superedge,

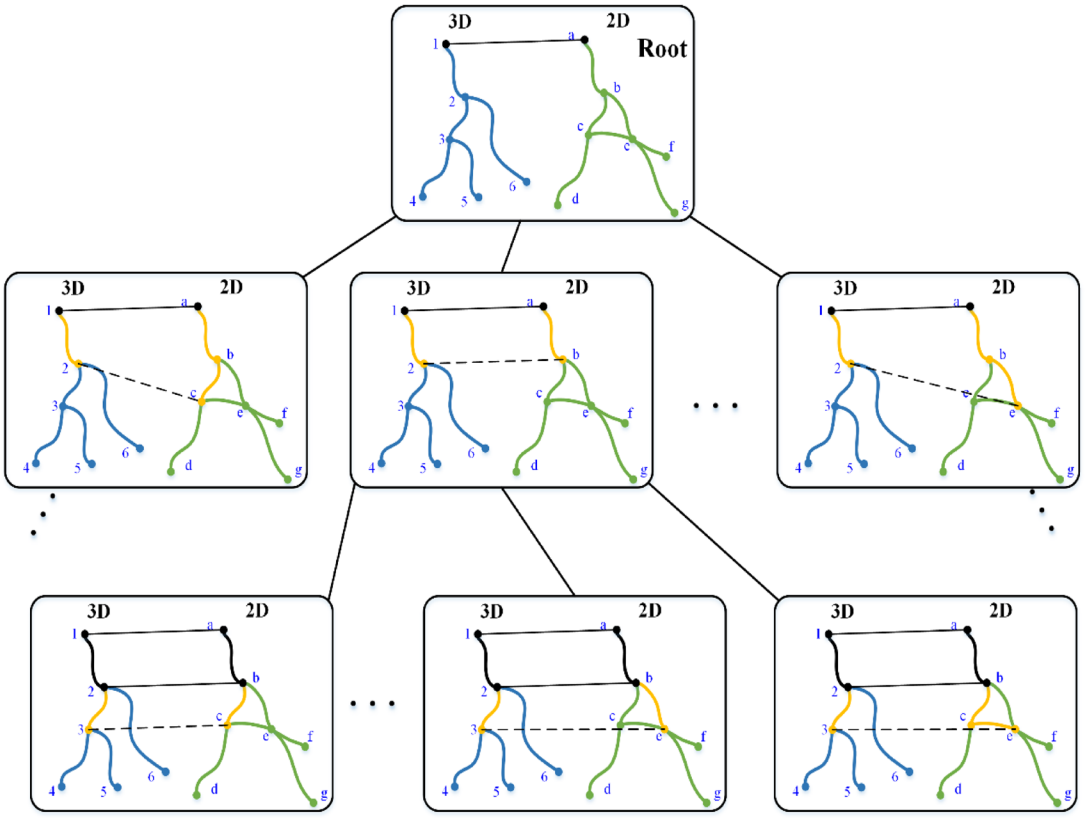

Figure 2. Partial search tree for vessel matching. A pair of vessel vertices is selected at the root node and then extended along the search tree. For the two vessel graphs in blue and green, matched edges are shown in black, and the newest candidate matching of edges is shown in yellow. Matched vertices are connected with a black solid line, and the newest candidate matching of vertices is connected with the black dashed line.

$$\widehat{T} = \underset{T,\pi^{\mathcal{E}}}{\operatorname{argmin}} \sum_{\left(e_i^{3D}, e_j^{2D}\right) \in \pi^{\mathcal{E}}} \mathcal{D}\left(P \circ T\left(e_i^{3D}\right), e_j^{2D}\right). \tag{2}$$

Hence, the registration problem can be transformed to solving both transformation T and matching $\pi^{\mathcal{E}}$.

2.2. Search tree

According to the formulation of $\pi^{\mathcal{E}}$, the matching of two graphs $\mathcal{G}^{3D}$ and $\mathcal{G}^{2D}$ can be formulated as a successive procedure by adding new superedge pair $\pi^{\mathcal{E}}_{(t+1)} = \pi^{\mathcal{E}}_{(t)} \cup \left(e_i^{3D}, e_j^{2D}\right)$. This property decomposes the matching procedure into successive states, and a search tree can be constructed using these states. To preserve the topological consistency, a new pair of superedges $\left(e_i^{3D}, e_j^{2D}\right)$ is feasible only if two conditions are satisfied: (a) the start-vertices of e_i^{3D} and e_j^{2D} are contained in the set of matched vertex pairs $\pi^{\mathcal{V}}_{(t)}$ and their end-vertices are excluded, and (b) no matched superedges overlap. This step can be described as feasible pairing detection, given the two graphs $\mathcal{G}^{3D}$ and $\mathcal{G}^{2D}$, current pairing of superedges and vertices, multiple new pairs of superedges $\left\{\left(e_{i_1}^{3D}, e_{j_1}^{2D}\right), \left(e_{i_2}^{3D}, e_{j_2}^{2D}\right), \ldots, \left(e_{j_k}^{3D}, e_{j_k}^{2D}\right)\right\}$ can be obtained. This step is formulated as function *FeasiblePairingDetection* $(\mathcal{G}^{3D}, \mathcal{G}^{2D}, \pi^{\mathcal{E}}_{(t)}, \pi^{\mathcal{V}}_{(t)})$ in algorithm 1. One example of a partial search tree is shown in figure 2, where a pair of vessel vertices is selected at the root node and expanded along the search tree.

In a newly expanded node of the search tree, the superedge pairing $\pi^{\mathcal{E}}$ is updated. The vertex pairing $\pi^{\mathcal{V}}$ determined by $\pi^{\mathcal{E}}$ is also updated. The new transformation T can be calculated by solving equation (2) with known$\pi^{\mathcal{E}}$. Furthermore, a score $\mathcal{S}$ related to the matching $\pi^{\mathcal{E}}$ and registration T will be calculated. The node $\mathcal{N}$ of the search tree can be formulated as $\mathcal{N} = \left\{\pi^{\mathcal{E}}, \pi^{\mathcal{V}}, T, \mathcal{S}\right\}$.

2.3. Transformation Calculation

Assuming that the superedge matching $\pi^{\mathcal{E}}$ is given, the transformation T can be obtained by using a closed-form solution. Dense matching of two vessel graphs is addressed by starting to conduct sparse correspondences between vertices and aligning edges/superedges between paired vertices by considering them as anchor points.

In this study, the dense correspondence π of edges/superedges can be estimated using uniform interpolation $\pi^{\mathcal{E}}$. This step is formulated as function $\pi_{(t+1)} \leftarrow \mathit{UniformInterpolation}\,(\pi^{\mathcal{E}}_{(t+1)})$ in algorithm 1.

For 3D points $\mathbf{C}^{3D}$ and 2D points $\mathbf{C}^{2D}$, the registration procedure can thus be reformulated as follows

$$\widehat{T} = \underset{T}{\operatorname{argmin}} \sum_{i} \left\| P \circ T\left(\boldsymbol{c}_i^{3D}\right) - \boldsymbol{c}_{\pi(i)}^{2D} \right\|, \tag{3}$$

where $\boldsymbol{c}_i^{3D}$ and $\boldsymbol{c}_j^{2D}$ are points on 3D and 2D vessel centerlines, π is associated with a mapping that assigns a 2D point to each 3D point, and $\pi\,(i) = j$ indicates that $\boldsymbol{c}_i^{3D}$ is matched with $\boldsymbol{c}_j^{2D}$. A fast closed-form solution (Ferraz *et al* 2014) is used here to obtain rigid transformation. The central idea of the closed-form solution is to formulate the coordinates of 3D points $\boldsymbol{c}_i^{3D}$ as weighted sums of four control points $\left\{\boldsymbol{u}_j^{(w)}\right\}$ in the world coordinate system denoted by superscript $^{(w)}$, $\boldsymbol{c}_i^{3D(w)} = \sum_{j=1}^{4} \alpha_{ij} \boldsymbol{u}_j^{(w)}$, with $\sum_{j=1}^{4} \alpha_{ij} = 1$. The corresponding coordinate information $\boldsymbol{c}_i^{3D(w)}$ can be retrieved from the virtual control points by recording the coefficient α_{ij}.

The purpose of finding a transformation that maps 3D points in the world coordinate system to the camera coordinate system, denoted by superscript $^{(c)}$, $T : \boldsymbol{c}_i^{3D(w)} \rightarrow \boldsymbol{c}_i^{3D(c)}$ is similar to that of finding a mapping of the virtual control points $T : \boldsymbol{u}_j^{(w)} \rightarrow \boldsymbol{u}_j^{(c)}$. This strategy transforms the problem of finding a best transformation to estimating the coordinates of the four control points $\left\{\boldsymbol{u}_j^{(c)}\right\}$ in the camera coordinate system. Given that the same coefficient relationship is held, we can obtain $\boldsymbol{c}_i^{3D(c)} = \sum_{j=1}^{4} \alpha_{ij} \boldsymbol{u}_j^{(c)}$. Supposing that each 3D point projection coincides with the corresponding 2D point, then we have $P \circ T\left(\boldsymbol{c}_i^{3D(w)}\right) = \boldsymbol{c}_{\pi(i)}^{2D}$. For $T\left(\boldsymbol{c}_i^{3D(w)}\right) = \boldsymbol{c}_i^{2D(c)}$, we derive:

$$\omega_i \begin{bmatrix} \boldsymbol{c}_{\pi(i)}^{2D} \\ 1 \end{bmatrix} = P\left(\boldsymbol{c}_i^{3D(c)}\right) = \mathbf{H} \sum_{j=1}^{4} \alpha_{ij} \boldsymbol{u}_j^{(c)}, \tag{4}$$

where $\mathbf{H}$is the internal calibration matrix of the camera, and ω_i is the homogeneous coefficient. The solution of $\left\{\boldsymbol{u}_j^{(c)}\right\}$ can be achieved by solving a small constant number of linear equations. Given the control points $\left\{\boldsymbol{u}_j^{(c)}\right\}$, the transformation $T : \boldsymbol{u}_j^{(w)} \rightarrow \boldsymbol{u}_j^{(c)}$ can be calculated by using the least-squares method (Arun *et al* 1987). The closed-form solution runs much faster than the optimization-based solutions, but it is slightly less accurate. Therefore, a refinement procedure is used to increase the accuracy at very low computational cost. A quasi-Newton algorithm is used to achieve the refinement of 3D transformation T by solving equation (3). The calculation of transformation step is formulated as the function $T \leftarrow \mathit{TransformationCalculation}\,(\pi)$ in algorithm 1.

2.4. Node Score

To evaluate the registration and matching of each node in the search tree, we define a score $\mathcal{S}$ related to the matching $\pi^{\mathcal{E}}$ and registration T. The score is based on two criteria. The first criterion corresponds to an expectation that more paired superedges with high accuracy are encouraged. Therefore, the score of the first criterion is defined as

$$\mathcal{S}_1\left(\pi^{\mathcal{E}}, T\right) = \sum_{\left(e_i^{A}, e_j^{B}\right) \in \pi^{\mathcal{E}}} e^{-d_F\left(P \circ T\left(e_i^{3D}\right), e_j^{2D}\right)/\sigma}, \tag{5}$$

where $d_F(\cdot)$ denotes the Fréchet distance (Alt and Godau 1995) of two sequential point sets, σ is the scale parameter to normalize the distance. $\mathcal{S}_1$ is related to the matching $\pi^{\mathcal{E}}$ and transformation T and its supremum is the counts of matched superedges $\left|\pi^{\mathcal{E}}\right|$. The second criterion corresponds to a common assumption on registration that more overlaps of projections of 3D points and 2D points are better. Thus, all the points are considered in the criterion and $\mathcal{S}_2$ is only related to the transformation T. Thus, we have

$$\mathcal{S}_2\,(T) = \frac{1}{\left|\mathbf{C}^{A}\right|} \sum_{i} e^{-\left(\min\limits_{j} \left\| P \circ T\left(\boldsymbol{c}_i^{3D}\right) - \boldsymbol{c}_j^{2D} \right\|\right)/\sigma} + \frac{1}{\left|\mathbf{C}^{B}\right|} \sum_{j} e^{-\left(\min\limits_{i} \left\| P \circ T\left(\boldsymbol{c}_i^{3D}\right) - \boldsymbol{c}_j^{2D} \right\|\right)/\sigma}, \tag{6}$$

where $\left|\mathbf{C}^{3D}\right|$ denotes the number of points in $\mathbf{C}^{3D}$. The supremum of $\mathcal{S}_2$ is 1. The minimal distance between projected 3D point $P \circ T\,(\boldsymbol{c}_i^{3D})$ and 2D point $\boldsymbol{c}_j^{2D}$ can be computed using distance transform. The overall score is defined as a weighted sum of the two scores

$$\mathcal{S}\left(\pi^{\mathcal{E}}, T\right) = \mathcal{S}_1\left(\pi^{\mathcal{E}}, T\right) + \alpha \mathcal{S}_2\,(T), \tag{7}$$

where α is the coefficient used to balance the contributions of $\mathcal{S}_1$ and $\mathcal{S}_2$. The calculation of node score is formulated as function $\mathcal{S} \leftarrow \mathit{NodeScore}(\pi^{\mathcal{E}}, T, \mathcal{P})$, where $\mathcal{P} = \{\sigma, \alpha\}$.

2.5. Greedy and Heuristic Strategy

To find the best state in the search tree effectively, two improved searching strategies are proposed. The first searching strategy, named greedy tree search, is an evolution of best-first search. The detailed pseudocode of greedy tree searching for 3D/2D registration (GTSR) is presented in algorithm 1. The 3D edge is regarded as a reference to match with 2D superedge. Thus, we first initialize the 2D superedge set $\mathcal{E}^{2D}$, which is defined as sequences of K consecutive edges (*Line 1*). The matching procedure starts with assigning an initial pairing of vertices (v_0^{3D}, v_0^{2D}) for the root node $\mathcal{N}^{(0)}$ (*Line 2*). However, this initial step is optional, indicating that the matching in the root node can be a null set. In that case, additional child nodes of null root node will be generated. The initial pairing of vertices can also be obtained automatically by choosing vertices with the maximal radius in 3D and 2D. In each level of the search tree, multiple new superedge pairings can be obtained by the feasible pairing detection. For each newly expanded child node, the superedge pairing $\pi^{\mathcal{E}}$, vertex pairing $\pi^{\mathcal{V}}$, transformation T and node score $\mathcal{S}$ are updated correspondingly (*Lines 15–18*).

The greedy strategy selects one best leaf node to expand the tree. However, the strategy has a limitation that it's easy to fall into the local extremum in the beginning steps, because fewer matched superedges are involved in estimating node score. In addition, less dense pairings of 3D and 2D points may decrease the accuracy of transformation calculation. We use a method in which more candidates are selected in the beginning L steps and then the greedy strategy begins with step $L+1$ (*Lines 9–10*). The procedure stops upon reaching the final level of the search tree, and the registration result $\widehat{T}$ is from the last leaf node (*Line 11*). The detailed implementation of the proposed GTSR method is presented in algorithm 1.

Algorithm 1. Greedy tree search for 3D/2D registration.

Input: 3D vessel graph $\mathcal{G}^{3D} = \{\mathcal{V}^{3D}, \mathcal{E}^{3D}\}$ and 2D vessel graph $\mathcal{G}^{2D} = \{\mathcal{V}^{2D}, \mathcal{E}^{2D}\}$, perspective projection operation P, initial vertex pairing v_0^{3D}, v_0^{2D};

Parameters: node score parameters $\mathcal{P} = \{\sigma, \alpha\}$, maximal length of superedge K, starting step of greedy strategy L;

Output: registration result $\widehat{T}$;

1 Initial 2D superedge set $\mathcal{E}^{2D}$, which is defined as sequences of K consecutive edges;

2 Create root node $\mathcal{N}^{(0)}$ with $\pi_0^{\mathcal{E}} =$ **null** and $\pi_0^{\mathcal{V}} = \{v_0^{3D}, v_0^{2D}\}$, leaf nodes list $Q^{(0)} = \{\mathcal{N}^{(0)}\}$;

3 **while** *isNotEmpty*$(Q^{(t)})$ **do**

4 **foreach** $\mathcal{N}^{(t)}$ **in** $Q^{(t)}$ **do**

5 $\left\{\left(e_{i_1}^{3D}, e_{j_1}^{2D}\right), \left(e_{i_2}^{3D}, e_{j_2}^{2D}\right), \ldots, \left(e_{i_k}^{3D}, e_{j_k}^{2D}\right)\right\} \leftarrow$*FeasiblePairingDetection*$(\ldots)$

6 **foreach** $\left(e_i^{3D}, e_j^{2D}\right)$ **in** $\left\{\left(e_{i_1}^{3D}, e_{j_1}^{2D}\right), \left(e_{i_2}^{3D}, e_{j_2}^{2D}\right), \ldots, \left(e_{i_k}^{3D}, e_{j_k}^{2D}\right)\right\}$ **do**

7 $\mathcal{N}^{(t+1)} \leftarrow$ *NodeExpand*$(\pi_{(t)}^{\mathcal{E}}, \left(e_i^{3D}, e_j^{2D}\right))$

8 $Q^{(t+1)} \leftarrow$ append $\mathcal{N}^{(t+1)}$

end foreach

end foreach

9 **if** $t > L$ **then**

10 $Q^{(t+1)} \leftarrow$ *GreedyStrategy*$(Q^{(t+1)})$;

end if

end while

11 Registration result $\widehat{T} = T_{(t)}$.

12 **function** *FeasiblePairingDetection*$(\mathcal{G}^{3D}, \mathcal{G}^{2D}, \pi_{(t)}^{\mathcal{E}}, \pi_{(t)}^{\mathcal{V}})$

13 **return** $\left\{\left(e_{i_1}^{3D}, e_{j_1}^{2D}\right), \left(e_{i_2}^{3D}, e_{j_2}^{2D}\right), \ldots, \left(e_{i_k}^{3D}, e_{j_k}^{2D}\right)\right\}$ // in section 2.2

14 **function** *NodeExpand*$(\pi_{(t)}^{\mathcal{E}}, \left(e_i^{3D}, e_j^{2D}\right))$

15 $\pi_{(t+1)}^{\mathcal{E}} = \pi_{(t)}^{\mathcal{E}} \cup \left(e_i^{3D}, e_j^{2D}\right), \pi_{(t+1)}^{\mathcal{V}} \leftarrow \pi_{(t+1)}^{\mathcal{E}}$;

16 $\pi_{(t+1)} \leftarrow$ *UniformInterpolation*$(\pi_{(t+1)}^{\mathcal{E}})$; // in section 2.3

17 $T_{(t+1)} \leftarrow$ *TransformationCalculation*$(\pi_{(t+1)})$; // in section 2.3

18 $\mathcal{S}_{(t+1)} \leftarrow$ *NodeScore*$(\pi_{(t+1)}^{\mathcal{E}}, T_{(t+1)}, \mathcal{P})$; // in section 2.4

19 **return** $\mathcal{N}^{(t+1)} = \left\{\pi_{(t+1)}^{\mathcal{E}}, \pi_{(t+1)}^{\mathcal{V}}, T_{(t+1)}, \mathcal{S}_{(t+1)}\right\}$

20 **function** *GreedyStrategy*$(Q^{(t)})$

21 **return** $Q^{(t)} = \left\{\text{argmax}_{\mathcal{N} \in Q^{(t)}}(\mathcal{S})\right\}$

The greedy strategy conducts a modified depth-first search that aims to reach the deepest level of the search tree, indicating that most paired superedges are obtained. The node score in the greedy strategy is applied for comparison among leaf nodes at the same level, and then the tree is pruned without backtracking. The second searching strategy, name heuristic tree search for 3D/2D registration (HTSR), is an evolution of the *A-star* search algorithm. Different from the greedy strategy, the heuristic tree search is adaptive and allows for backtracking. It maintains a heuristic queue Q_h of tree nodes that is most likely to lead to a correct solution. Furthermore, a close queue Q_c is used to record visited nodes.

The pseudocode of HTSR is presented in algorithm 2. It begins with the initialization of 2D superedges and root node (*Lines 1–2*). Then the heuristic queue is initialized by pushing the root node into it, and the close queue is initialized as a null set (*Line 3*). For the visited node $\mathcal{N} = \left\{\pi^{\mathcal{E}}_{(t)}, \pi^{\mathcal{V}}_{(t)}, T_{(t)}, \mathcal{S}\right\}$, multiple new superedge pairings can be obtained by the feasible pairing detection (*Line 6*). For each new pair of superedges, a new expanded child node $\mathcal{N}^{(t+1)}$ can be constructed by updating the superedge pairing $\pi^{\mathcal{E}}$, vertex pairing $\pi^{\mathcal{V}}$, transformation T and node score $\mathcal{S}$ correspondingly (*Line 8*). The new expanded child nodes are pushed into the heuristic queue, and the queue is sorted in descending order based on the node score (*Line 9*). The iteration procedure stops when the heuristic queue Q_h is empty or the capacity of close queue Q_c is above M (*Line 4*). The final registration result T is obtained from the close queue, for which the node score is the highest. Detailed implementation of the proposed HTSR method is presented in the following pseudocode.

Algorithm 2. Heuristic tree search for 3D/2D registration.

Input: 3D vessel graph $\mathcal{G}^{3D} = \{\mathcal{V}^{3D}, \mathcal{E}^{3D}\}$ and 2D vessel graph $\mathcal{G}^{2D} = \{\mathcal{V}^{2D}, \mathcal{E}^{2D}\}$, perspective projection operation P, initial vertex pairing v_0^{3D}, v_0^{2D};

Parameters: node score parameters$\mathcal{P} = \{\sigma, \alpha\}$, maximal length of superedge K, maximum counts of iterations M;

Output: registration result $\widehat{T}$;

1 Initial 2D superedge set $\mathcal{E}^{B}$, which is defined as sequences of K consecutive edges;

2 Create root node $\mathcal{N}^{(0)} = \left\{\pi_0^{\mathcal{E}}, \pi_0^{\mathcal{V}}\right\}$ with $\pi_0^{\mathcal{E}} = \text{null}$ and $\pi_0^{\mathcal{V}} = \{v_0^{3D}, v_0^{2D}\}$.

3 Initialize heuristic queue $Q_h \leftarrow \text{Push}\ (\mathcal{N}^{(0)})$ and close queue $Q_c = \text{null}$

4 **while** *isNotEmpty*(Q_h) & $|Q_c| < M$ **do**

5 $\quad\mathcal{N} \leftarrow \text{Pop}\ (Q_h)$, $Q_c \leftarrow \text{Push}\ (\mathcal{N})$;

6 $\quad\left\{\left(e_{i_1}^{3D}, e_{j_1}^{2D}\right), \left(e_{i_2}^{3D}, e_{j_2}^{2D}\right), \ldots, \left(e_{i_k}^{3D}, e_{j_k}^{2D}\right)\right\} \leftarrow$*FeasiblePairingDetection*$(\ldots)$

7 $\quad$**foreach** $\left(e_i^{3D}, e_j^{2D}\right)$ **in** $\left\{\left(e_{i_1}^{3D}, e_{j_1}^{2D}\right), \left(e_{i_2}^{3D}, e_{j_2}^{2D}\right), \ldots, \left(e_{i_k}^{3D}, e_{j_k}^{2D}\right)\right\}$ **do**

8 $\quad\quad\mathcal{N}^{(t+1)} \leftarrow$. *NodeExpand*$(\pi^{\mathcal{E}}_{(t)}, \left(e_i^{3D}, e_j^{2D}\right))$

9 $\quad\quad Q_h \leftarrow$ *PushAndDescendSort*$(\mathcal{N}^{(t+1)})$

$\quad$**end foreach**

end while

10 Registration result $\widehat{T} = \text{argmax}_{\{\pi^{\mathcal{E}}, \pi^{\mathcal{V}}, T, \mathcal{S}\} \in Q_c}\ \{\mathcal{S}\}$.

The complexity analysis of two methods are presented. In practice, the 3D vessel edges are traversed and multiple 2D superedges are selected to match with each 3D edge. Therefore, the depth of search tree can be specified as the capacity of 3D edge set $d = |\mathcal{E}^{3D}|$. The branch factor of the search tree can be defined as the counts of *FeasiblePairingDetection* outputs whose maximum is specified as $b = 2^K - 1$, where K is the maximal length of superedge. The time complexities of functions *NodeScore* and *TransformationCalculation* are both $O(n)$, where n denotes the counts of paired points. Therefore, the time complexity of *NodeExpand* is $O(n)$. Considering the iterative procedure, the time complexities of GTSR and HTSR are $O((b^L + d - L)\, n)$ and $O(Mn)$, respectively. It can be found that the computation time of GTSR is sensitive to L and K, while HTSR is more stable.

3. Experiments and results

3.1. Experimental Setting

The 3D/2D registrations are evaluated by calculating the mean projected distance (mPD) (van de Kraats *et al* 2005) between projected 3D and 2D centerline points. The performance of the proposed 3D/2D registration methods is compared with four comparative methods in each experiment. (1) An extension of ICP (Besl and McKay, 1992) (i.e. ICP-BP) to the 3D/2D application introduced in Baka *et al* (2014). (2) An accelerated method for ICP matching (i.e. DT) (Rivest-Henault *et al* 2012) uses a precomputed distance transformation of

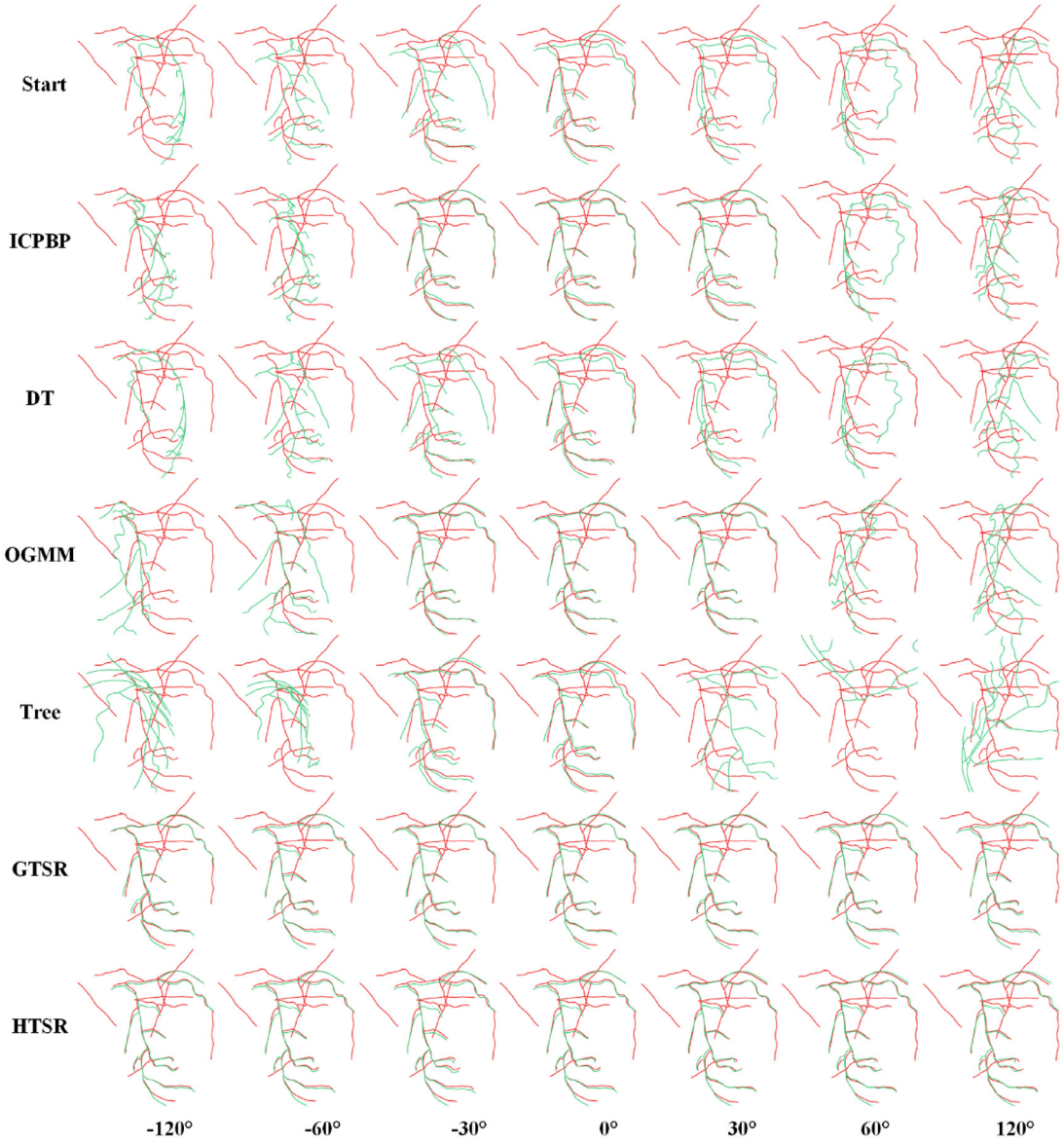

Figure 3. Results of pose independence experiment of the proposed method and comparative methods. Projected 3D and 2D centerlines are shown in green and red, respectively. The vessels of the initial state are presented in the first row. In the remaining rows from up to down, the results of ICPBP, DT, OGMM, Tree, GTSR and HTSR are presented. In the columns from left to right, the rotation angles of the 3D vessel are set to −120°, −60°, −30°, 0°, 30°, 60° and 120°.

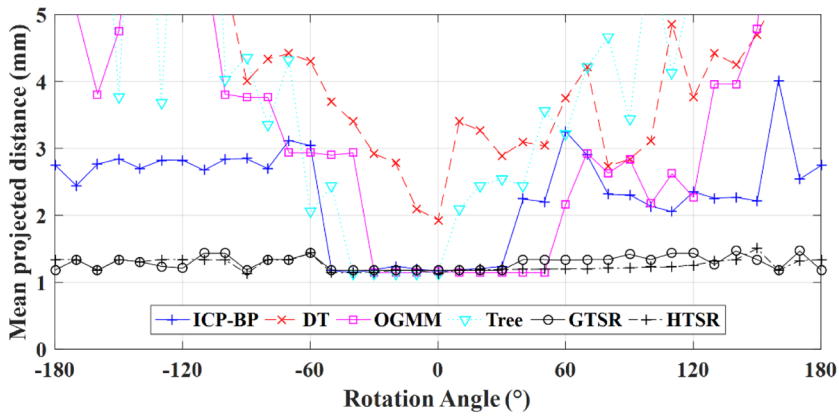

Figure 4. Distance errors of pose independence experiment. The *X*-axis shows the rotation angles from −180° to 180°. The *Y*-axis indicates the mean projected distance from 0 to 5 mm. The results of the proposed method and comparative methods are presented.

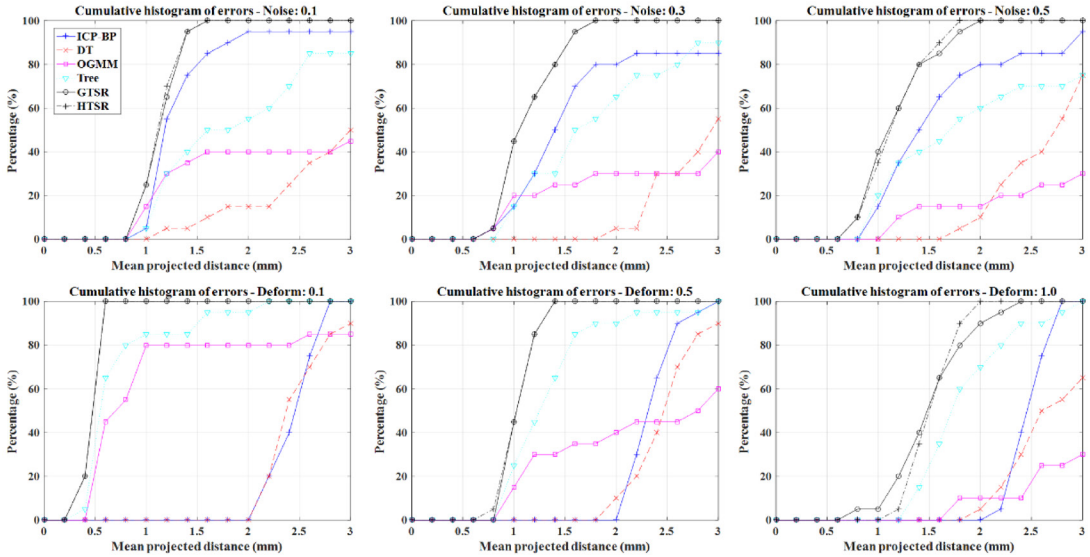

Figure 5. Cumulative histogram of errors of the XCAT data experiment. The percentage is indicated by the *Y*-axis and 100% percentage indicates 80 instances of registration. Mean projected distance (unit: mm) is indicated by the *X*-axis.

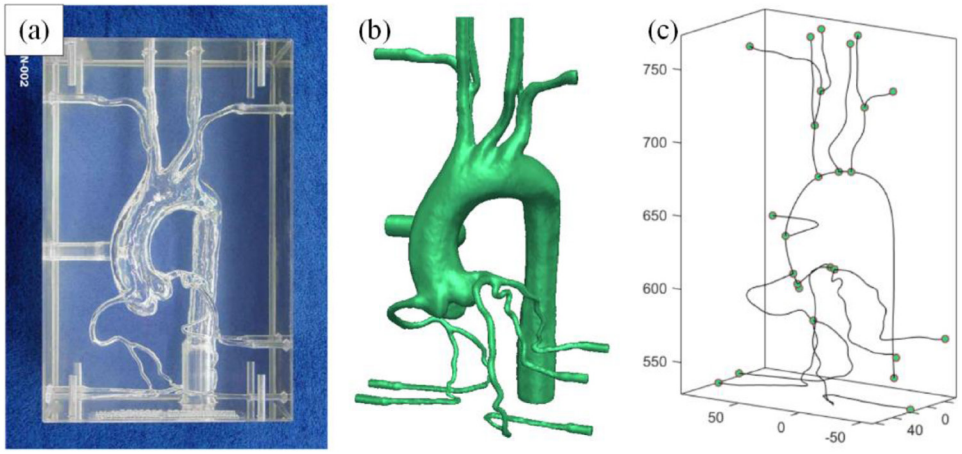

Figure 6. Aorta model used in this work. (a) Normal aortic arch model. (b) Segmented vessel model. (c) Extracted 3D vessel graph.

a segmented vessel tree. (3) Tree topology matching for 3D/2D registration (i.e. Tree) (Benseghir *et al* 2015). (4) Oriented Gaussian mixture models (OGMM) (Baka *et al* 2014).

The node score parameters σ and α for proposed GTSR and HTSR are selected empirically. The scales of position and orientation are set $\sigma = 5$, and $\alpha = 0.2$ is used to balance the contributions of the two score items. The length of superedge $K = 3$ is applied to extract superedge sets. In GTSR, the greedy strategy starts at step $L = 3$. For HTSR, M determines the maximum counts of iterations. M is set according to the node counts N of graphs to be registered. For $N < 15$, $M = 100$. is sufficient for the tree search. For $15 < N < 25$, $M = 200$ is selected. For $N > 25$, a maximum count of $M = 300$ is selected.

3.2. Validation of Proposed Method

Empirical assessments of the GTSR and HTSR are presend in this section. Since the vessel matching in the proposed method relies on the topological continuity of vessels, the proposed method is sensitive to the disconnected vessel centerlines. For noisy vessel branch, the proposed method shows good robustness.

The size of coronary branches, which can be defined as the capacity of edge set $|\mathcal{E}|$, also influences the registration. For vessel matching based on topology continuity, $|\mathcal{E}| \geqslant 3$ is recommended to establish a proper registration. However, $|\mathcal{E}|$ determines the depth of search tree. Large size of coronary branches means that more trails are required to find the optimal result. In spite of this, the registration of 3D and 2D vessels is executed using the whole vessel branch, which represents complete topological information. The initial vertex pairing is crucial for the proposed method, the search tree expands from the root node. If the root node is wrong, such as incorrect pairing, the vessel matching will fail. If the initial vertex pairing is not given, the search tree will start with a null

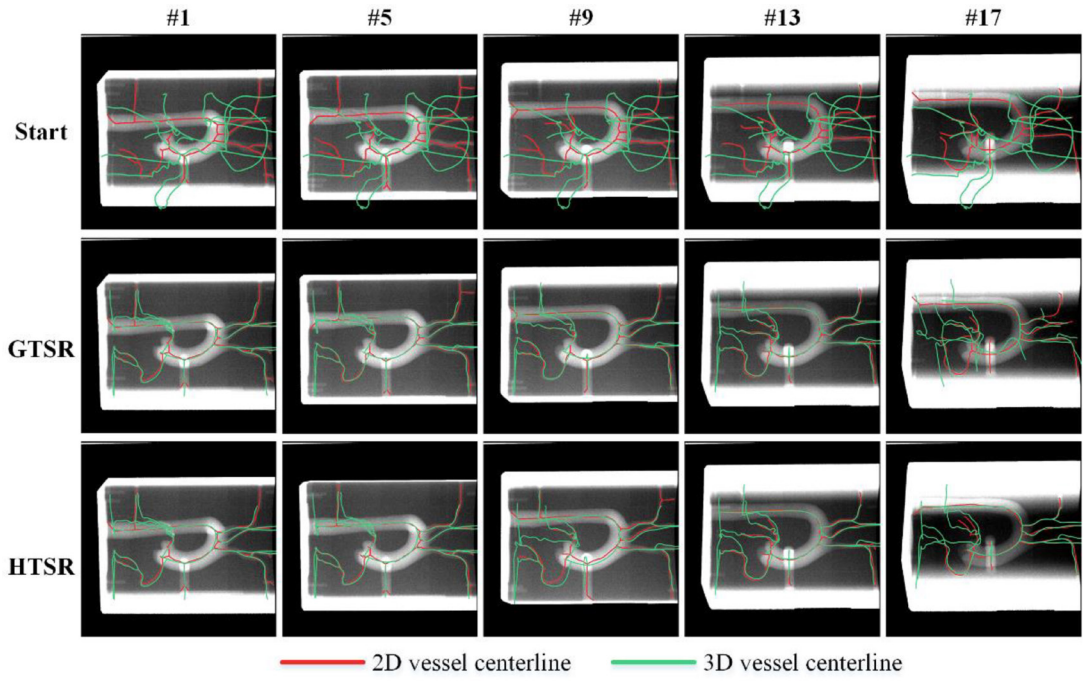

Figure 7. Results of aorta model experiments. Projected 3D and 2D centerlines are shown in green and red, respectively. The vessels of the initial state are presented in the first row. Results of GTSR and HTSR methods are presented in the second and third rows, respectively. Frames of Nos. 1, 5, 9, 13 and 17 are shown from left to right.

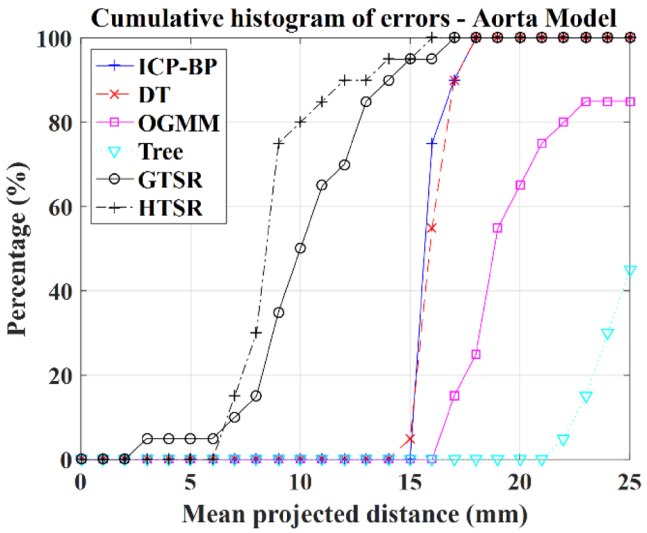

Figure 8. Cumulative histogram of errors of the aorta model experiment. The percentage is indicated by the *Y*-axis and 100% percentage indicates 80 instances of registration. Mean projected distance (unit: mm) is indicated by the *X*-axis.

root and multiple leaf nodes with candidate vertex pairing are generated. Thus, the time complexities of GTSR and HTSR will be multiplied by $|\mathcal{V}^{2D}|$.

The initial pose, noise and deformation are mainly concerned in the validation. A public available dataset, XCAT data (Segars *et al* 2010), is applied to validate the pose independence and robustness to errors. A set of dynamic volume data of chests with heart-beat motions is generated from the XCAT tools. The entire heart tissue, coronary arteries, and aorta are involved and enhanced. The volume data contain 301 slices, and the slice spacing is 0.5 mm. The image size and pixel spacing of each slice are 400 × 400 and 0.5 mm × 0.5 mm. The volume data are input into the medical image processing software (*Materialise Mimics*), and then extract the centerlines and connectivity relation of coronary arteries.

Given the 3D vessel graph $\mathcal{G}^{3D}$, a dataset of simulated 2D centerlines with noise and non-rigid deformation is designed, similar to the simulation in Serradell *et al* (2011). The deformation of the vessel is simulated using the statistical shape model (SSM), which can be constructed using the dynamic 3D centerlines. The SSM is estab-

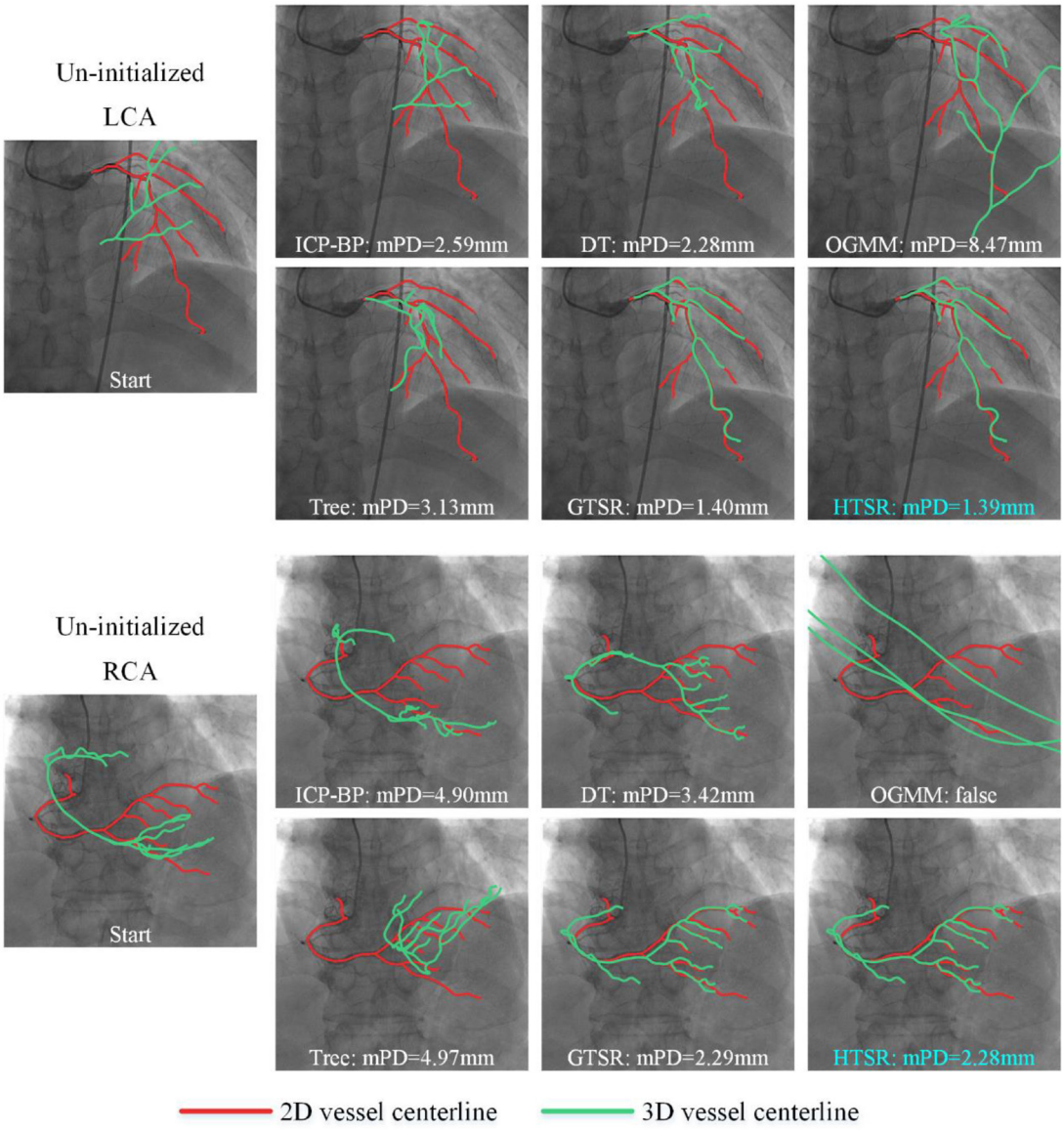

Figure 9. Results of 3D/2D registration methods conducted on un-initialized coronary artery data. Two samples of LCA and RCA are presented at the top and bottom of the figure, respectively. The applied method and mPD (unit: mm) are presented below the respective plotted sub-figures. Projected 3D and 2D centerlines are shown in green and red. The texts of registration with the best accuracy are colored in light blue.

lished to retain 95% of the variance, resulting in approximately 20 parameters. The deformed 3D vessel can be expressed as $\mathcal{T}(\mathcal{G}^{3D}, \boldsymbol{b})$, where $\mathcal{T}$ denotes the non-rigid deformation driven by SSM and $\boldsymbol{b}$ is the parameter vector of constructed SSM. Then the 3D vessel structure is projected onto a 2D plane defined by the camera internal matrix from a DICOM file of XRA, to obtain the simulated 2D vessel structure $P \circ \mathcal{T}(\mathcal{G}^{3D}, \boldsymbol{b})$. Branch noises are randomly added to the 2D centerline by locating randomly generated free-form curves adjacent to the 2D vessel branch, implying that the topology of the 2D vessel is changed and different with a 3D centerline. Finally, the simulated 2D vessels are expressed as $P \circ \mathcal{T}(\mathcal{G}^{3D}, \boldsymbol{b}) + \mathcal{N}(\beta)$, where $\mathcal{N}(\beta)$ denotes that β percentage of points are added. Furthermore, rotated 3D vessels are produced $T(\mathcal{G}^{3D}, \boldsymbol{\theta})$, where T denotes rigid transformation and $\boldsymbol{\theta}$ denotes rotation angles.

3.2.1. *Pose independence*

The proposed method is designed with a large capture range, and the simulation experiment aims to test the ability to align 3D vessels rotated with an arbitrary angle to deformed and noisy 2D vessels. In this experiment, 3D vessels $T(\mathcal{G}^{3D}, \boldsymbol{\theta})$ are registered to the deformed and noisy 2D vessels $P \circ \mathcal{T}(\mathcal{G}^{3D}, \boldsymbol{b}) + \mathcal{N}(\beta)$. We set the rotation angle range from $-180°$ to $180°$ with $10°$ interval and produce 36 cases of 3D vessels. The deformation parameter is set as $\boldsymbol{b} = 0.1\boldsymbol{\lambda}$, where $\boldsymbol{\lambda}$ is the eigen-vector of SSM; the noise percentage is set as $\beta = 50\%$.

Results of the pose independence experiment are visualized by plotting centerlines and distance error curves, as presented in figures 3 and 4. Projected 3D and 2D centerlines are shown in green and red in figure 3, respec-

tively. The results of rotation angles $-120°$, $-60°$, $-30°$, $0°$, $30°$, $60°$, and $120°$ are selected. Accordingly, the distance errors of simulation experiments are presented in figure 4. Examples and distance error indicate that the proposed GTSR and HTSR methods are insensitive to initial pose. They achieve average accuracies of 1.29 and 1.25 mm on the whole rotation angles, respectively. These comparative methods perform well on the data with rotation from approximately $-30°$ to $30°$. By contrast, for rotation angles larger than $30°$, the distance errors increase rapidly.

3.2.2. Robustness to errors

Two sets of vessel data are generated for the robustness validation experiment. The first set is aim to validate the robustness to noise. Slighted deformation and small rotation are added. The deformation parameter is set as $\boldsymbol{b} = 0.1\boldsymbol{\lambda}$, and rotation angles $\boldsymbol{\theta}$ are randomly generated ranging from $-10°$ to $10°$. Three noise parameters $\{\beta\} = \{10\%, 30\%, 50\%\}$ are applied to the 2D vessels. The second set is aim to validate the robustness to deformation. Small rotation $-10° \leqslant \boldsymbol{\theta} \leqslant 10°$ and slighted noise $\beta = 10\%$ are added to vessel data. Three deformation parameters $\{\boldsymbol{b}\} = \{0.1\boldsymbol{\lambda}, 0.5\boldsymbol{\lambda}, 1.0\boldsymbol{\lambda}\}$ are applied to the 2D vessels. 20 samples are generated for each set of parameters, and each sample is performed 4 times for every 3D/2D registration method. Results of the robustness validation experiment are displayed by the cumulative histogram of errors, as shown in figure 5. It can be found that the accuracy decrease obviously with the noise and deformation increase. For all the comparative methods, the proposed method demonstrated to be very robustness with respect to different noise and deformation. It is obvious that the proposed method is more accurate than the other comparing methods.

3.3. Aorta model experiment

An aorta model is applied to produce a dataset for 3D/2D registration. The size of the model is 26 cm × 17 cm × 14 cm. The model corresponds to the normal aortic arch model with the left and right coronary (*www.elastrat.com*), as shown in figure 6(a). A Siemens SOMATOM Definition Flash CT is used to scan the model and derive the corresponding volume data, which contains 316 slices with 1 mm spacing between slices. The image size of one slice is 512 × 512, and pixel spacing is 0.590 mm × 0.590 mm. Medical image processing software (*Materialise Mimics*) is used to segment the vessel, and the segmented vessel model is shown in figure 6(b). With the centerline points and connectivity relations, the 3D vessel graph can be constructed, as shown in figure 6(c).

A rotational C-arm device is likewise used to produce rotational x-ray images. One image frame is captured when the C-arm rotates 2.5°, and a total of 20 frames are acquired. The image size and pixel spacing of x-ray image are 1024 × 1024 and 0.417 mm × 0.417 mm respectively. The x-ray images of the aorta model are segmented manually, and then the 2D centerlines are extracted using image thinning. The 2D graphs can be obtained on the basis of neighbor relations.

Initial vertex pairings for aorta graphs are manually labeled. The 3D aorta graph is registered to the 20 frames of the 2D graph. Each frame is performed four times; thus, 80 instances of registration are conducted for each method. The results of the aorta model experiment are visualized by centerlines and cumulative histograms, as presented respectively in figures 7 and 8. The frames of Nos. 1, 5, 9, 13, and 17 are selected to be displayed from left to right. The first row indicates the initial pose of the projected 3D and 2D vessels. The second and third rows indicate the results of GTSR and HTSR, respectively. The results in figure 7 present a good overlap of 3D and 2D vessels. Detailed statistical errors are presented in figure 8 in the form of a cumulative histogram of errors. The errors are computed using the mean projected distance (unit: mm). The GTSR and HTSR methods achieve accuracies of 10.16 and 8.83 mm, respectively, which are tolerable with respect to the size of the aorta model. The four comparative methods, ICP-BP, DT, OGMM, and Tree, achieve accuracies of 15.91, 15.95, 19.92, and 26.85 mm, respectively.

3.4. Clinical experiment of coronary arteries

Clinical data of coronary arteries are used in this study. The coronary artery dataset consists of intra-operation CTA and XRA coronary images from 14 patients from Peking Union Medical College Hospital. A total of 30 pairs of 3D and 2D vessel data are used, comprising 16 pairs of right coronary arteries (RCA) and 14 pairs of left coronary arteries (LCA). The CTAs are acquired on a Siemens SOMATOM Definition Flash CT, reconstructed in the arterial phase. The image size and pixel spacing of each slice are 512 × 512 and approximately 0.35 mm × 0.35 mm, respectively. The scanning range of the collected CTAs covers all the cardiac tissue. The number of slices ranges from 200 to 400, and the slice spacing is 0.75 mm. The XRAs are acquired on a Philips INTEGRIS Allura Flat Detector at a frame rate of 15 fps. The image size and pixel spacing of the sequences are 512 × 512 and 0.37 mm × 0.37 mm, respectively.

CTAs of coronary arteries are preprocessed using medical image processing software (*Materialise Mimics*) manipulated by doctors. The 3D centerlines and connectivity of vessel branches can be acquired from the software outputs. For XRA sequence, one frame with full filled contrast agent is selected manually and segmented

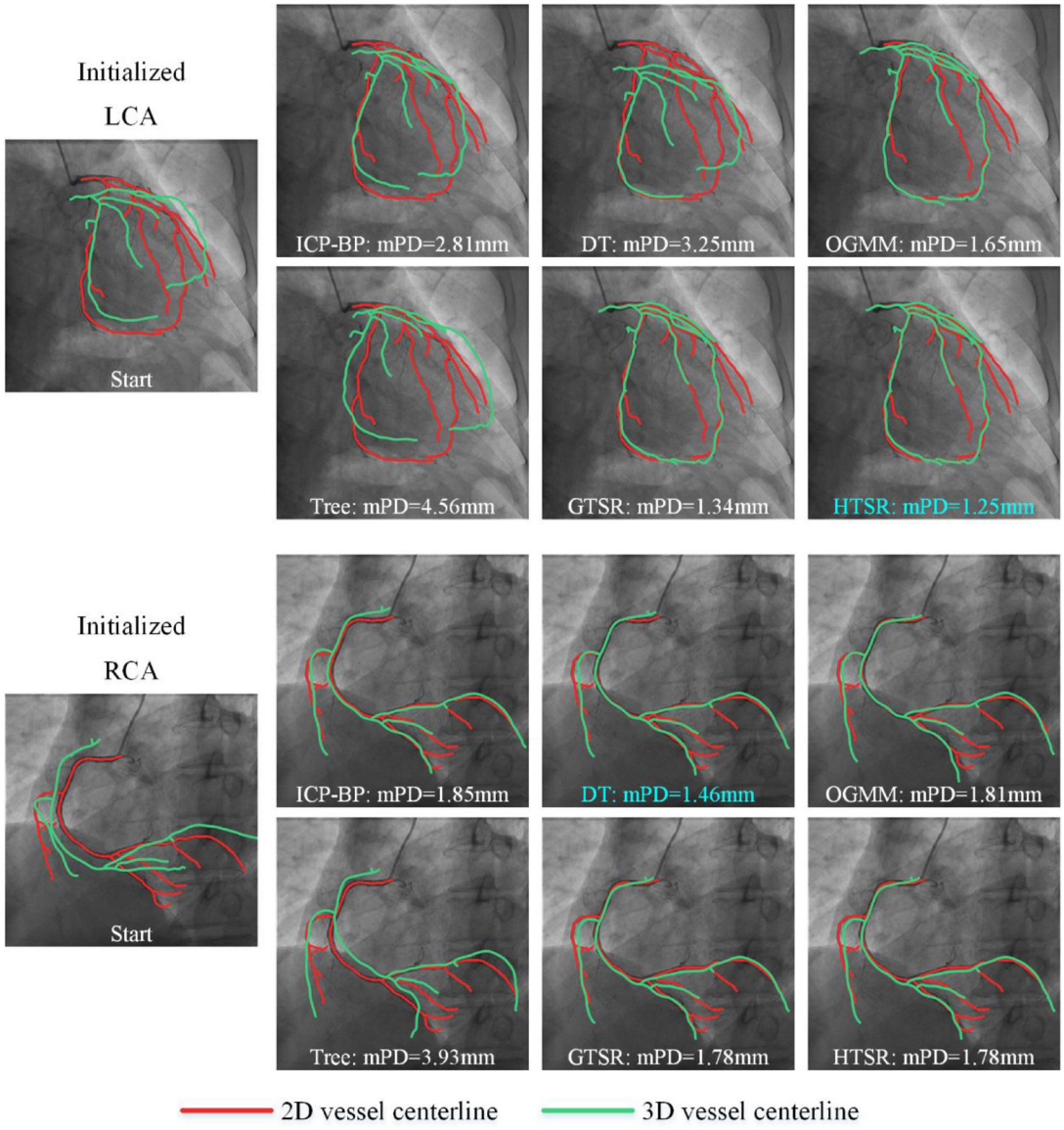

Figure 10. Results of 3D/2D registration methods performed on initialized coronary artery data. Two samples of LCA and RCA are presented at the top and bottom of the figure, respectively. The applied method and mPD (unit: mm) are presented below the respective plotted sub-figures. Projected 3D and 2D centerlines are shown respectively in green and red. The texts of registration with the best accuracy are colored in light blue.

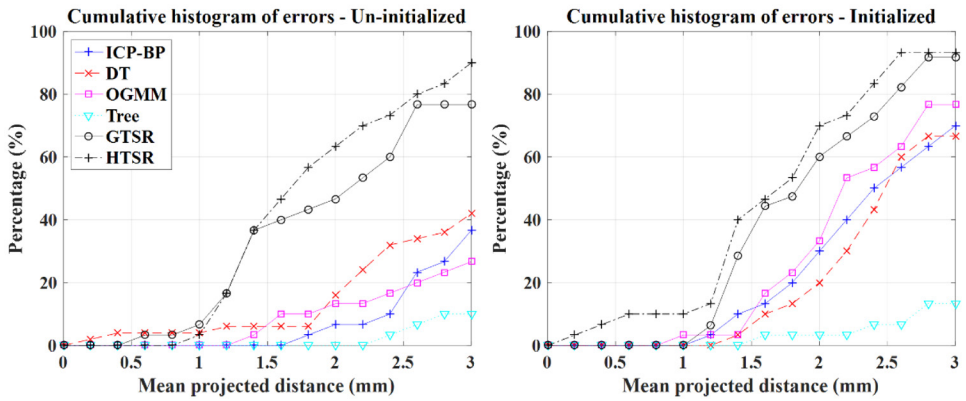

Figure 11. Cumulative histograms of errors of un-initialized and initialized clinical experiments. Percentage is indicated by the *Y*-axis, and 100% percentage indicates 120 instances of registration. Mean projected distance (unit: mm) is indicated by the *X*-axis.

Table 2. Statistical results of all methods on three datasets used in this work.

	XCAT simulation data	Aorta model data	Clinical data of coronary arteries		
			Distance error (mm)		Computation time (s)
	Distance error (mm)	Distance error (mm)	Un-initialized	Initialized	
ICP-BP	2.30 (±0.73)	15.91 (±0.81)	5.78(±1.94)	2.95(±1.95)	0.43 (±0.09)
DT	4.26 (±1.28)	15.95 (±0.80)	5.06(±3.06)	3.10(±2.12)	**0.06 (±0.01)**
OGMM	3.60 (±2.21)	19.92 (±3.31)	8.75(±3.00)	2.65(±1.47)	10.39 (±5.49)
Tree	5.66 (±4.59)	26.85 (±5.08)	7.03(±3.91)	3.41(±1.85)	14.21 (±5.48)
GTSR	1.29 (±0.10)	10.16 (±3.18)	2.16(±1.66)	2.07(±0.74)	9.48(±6.17)
HTSR	**1.25 (±0.09)**	**8.83 (±2.23)**	**1.85(±0.71)**	**1.79(±0.87)**	2.28 (±0.30)

using a convolutional neural network based method (Nasr-Esfahani *et al* 2018). Then, centerlines are extracted by applying iterative filtering operation and multi-direction indexed non-maximum suppression. Then, an eight-neighborhood tracking method is used to connect adjacent 2D points. With the centerlines and the connection information, 3D and 2D graphs can be constructed. Vessel segmentation, centerline extraction, and graph construction can be replaced with other methods. In the experiment, all the centerline-based comparative methods are conducted with the same centerline information.

The node counts of 3D vessel graphs range from 8 to 23, and the numbers of sampled 3D vessel points are approximately 500 for coronary arteries. The node counts of 2D vessel graphs range from 22 to 35, and the numbers of sampled 2D vessel points are approximately 1000. Initial vertex pairings for coronary graphs are automatically recognized by selecting the vertices with the maximum radius.

In the clinical experiment, the initial projection of the 3D vessel onto the 2D image plane is far from the 2D vessel and exhibits large rotation angle discrepancies. For pose initialization-dependent methods, although the translation between 3D and 2D data can be adjusted by an automatic normalization operation, these methods predictably result in failed registration in most instances. Therefore, the initial pose for each 2D vessel is manually adjusted to conduct 3D/2D registration on un-initialized and initialized data. The mean value and standard deviation of distance errors (mPD) of un-initialized data are 15.17 and 7.35 mm, respectively. After initialization, the mean value and standard deviation are 5.70 mm and 3.14 mm, respectively. The proposed method aims to find matching and then calculate the transformation on the basis of topological consistency and dense matching of vessel points, respectively. The proposed method is expected to perform well on un-initialized and initialized data.

Four trials of registration are conducted for each pair of 3D and 2D vessels, and 120 instances of registration are conducted for each method. Samples of 3D/2D registration methods performed on un-initialized and initialized coronary artery data are presented in figures 9 and 10 in the form of centerlines overlapped on the x-ray images, respectively. The applied method and distance error are shown at the bottom of the respective plotted sub-figures. For the un-initialized data, only the GTSR and HTSR methods can achieve satisfactory results. For the initialized data, most comparative methods can register 3D and 2D data. The proposed method still performs best. The corresponding cumulative histograms of errors are presented in figure 11. For the initialized data, the percentages of distance errors under 3 mm of these methods are 36.67%, 41.67%, 26.67%, 10%, 76.67%, and 90%. For the un-initialized data, the corresponding percentages are 70.00%, 66.67%, 76.67%, 13.33%, 93.33%, and 96.67%.

Table 2 presents the detailed statistical results of registration errors and the computation times of all the methods. The average and standard deviations are calculated. In the table, the best performances on accuracy and computational efficiency are in bold. The codes are run on a PC (Intel I7-7700 CPU, MATLAB platform), and the parameter tuning of all the methods aims to obtain high accuracy. The implementations of the algorithm presented in this paper are available online at https://github.com/JianjunZhu/HTSR.

4. Discussion

In this study, a tree search framework for 3D/2D registration of un-initialized vessel graphs is proposed. On the basis of the property that the matching procedure can be decomposed into successive states, the registration problem is transformed into a tree search problem. Dense matching of the vessel points and closed-form transformation are used to obtain the registration results. Then, the node scores used to evaluate the qualities of matching and registration are calculated. Based on a definition, an HTSR is proposed to find the optimal registration with the highest score in the search tree. Given that the matching is based on the topological continuity of 3D and 2D vessels, the proposed method is expected to be insensitive to the initial pose.

Four state-of-art methods, namely, ICP-BP (Besl and McKay 1992), DT (Rivest-Henault *et al* 2012), OGMM (Baka *et al* 2014) and Tree (Benseghir *et al* 2015), are compared with our methods in the experiments. In addition, the GTSR approach that uses greedy search strategies as the baseline is proposed. The XCAT simulation experiment is designed to test the robustness with respect to the initial pose, noise and deformation. The results of simulated data demonstrate that the proposed method is barely sensitive to the initial pose even with disturbance of noise and deformation. Real captured images are used in the aorta model experiment and clinical coronary artery experiment. For un-initialized data, only the proposed method can achieve acceptable registration results. For the data provided with post initialization, our method continues still achieve the best registration accuracy among these 3D/2D registration methods.

Among these methods, the proposed GTSR and HTSR can align data with large-scale rigid transformation. ICP-BP and DT achieve similar accuracies because they use the closest relationship to estimate the similarity metric. Given that DT precomputes a distance transform of the 2D centerline, it performs the fastest among all the methods, achieving an average computation time of 0.06 s for clinical data. OGMM performs well on simulated data with low rotation difference, from approximately $-30°$ to $30°$. By contrast, OGMM performs poorly on data with large rotation and un-initialized data because the optimization-based method relies on the initial pose. Tree methods use the topology continuity of vessels to obtain accurate matching. The distance-based metric is used to pair the vessel branches; consequently, it is sensitive to initial pose. The HTSR uses a global informed searching strategy, which performs better than the GTSR based on local greedy strategy in all experiments.

5. Conclusions

We presented a novel and potentially clinically useful 3D/2D registration method of un-initialized vessel graphs based on heuristic tree search. Insensitivity to the initial pose of registration is the primary advantage of our method. Moreover, GTSR and HTSR are robust to noise and deformation and their computation times are acceptable and improvable. Thus, it is suitable to navigate vascular intervention for clinical practice. One major limitation of the proposed method is that the topology of vessel centerlines is mandatory requirement. Hence, the accuracy of the proposed method relies on the XRA images preprocessing, including vessel segmentation, centerline extraction, and topology construction.

Acknowledgments

This work was supported by the National Key Research and Development Program of China (2017YFC0107900), National Science and Technology Major Project of China (2018ZX10723-204-008), and the National Science Foundation Program of China (61971040, 81627803, 61771056, 61527827, 61901031).

Authors' contributions

ZJJ, FJF, GS and YJ conceived and conducted the experiments; ZJJ and YJ analyzed the results and wrote the paper; ADN, SH, WC, ZSJ and YJ reviewed the manuscript and provided many thoughtful suggestions to improve the manuscript.

Conflict of interest

The authors declare that they have no competing interests.

Ethical statement

All procedures performed in studies involving human participants were in accordance with the ethical standards of the institutional and/or national research committee and with the 1964 Helsinki declaration and its later amendments or comparable ethical standards. Informed consent was obtained from all individual participants included in the study.

ORCID iDs

Shoujun Zhou https://orcid.org/0000-0003-3232-6796
Jian Yang https://orcid.org/0000-0003-1250-6319

References

Alt H and Godau M 1995 Computing the Fréchet distance between two polygonal curves *Int. J. Comput. Geom. Appl.* **5** 75–91

Arun K S, Huang T S and Blostein S D 1987 Least-squares fitting of two 3D point sets *IEEE Trans. Pattern Anal. Mach. Intell.* **5** 698–700

Baka N, Metz C T, Schultz C J, Geuns R V, Niessen W J and Walsum T V 2014 Oriented gaussian mixture models for nonrigid 2D/3D coronary artery registration *IEEE Trans. Med. Imaging* **33** 1023–34

Benseghir T, Malandain G and Vaillant R 2013 Iterative closest curve: a framework for curvilinear structure registration application to 2d/3d coronary arteries registration *Int. Conf. on Medical Image Computing and Computer-Assisted Intervention* (Berlin: Springer) pp 179–86

Benseghir T, Malandain G and Vaillant R 2015 A tree-topology preserving pairing for 3D/2D registration *Int. J. Comput. Assist. Radiol. Surg.* **10** 913–23

Besl P J and McKay N D 1992 A method for registration of 3D shapes *IEEE Trans. Pattern Anal. Mach. Intell.* **14** 239–56

Dorgham O M, Laycock S D and Fisher M H 2012 GPU accelerated generation of digitally reconstructed radiographs for 2D/3D image registration *IEEE Trans. Biomed. Eng.* **59** 2594–603

Fan J, Yang J, Ai D, Xia L, Zhao Y, Gao X and Wang Y 2016a Convex hull indexed Gaussian mixture model (CH-GMM) for 3D point set registration *Pattern Recogn.* **59** 126–41

Fan J, Yang J, Lu F, Ai D, Zhao Y and Wang Y 2016b 3-Points Convex Hull Matching (3PCHM) for fast and robust point set registration *Neurocomputing* **194** 227–40

Ferraz L, Binefa X and Moreno-Noguer F 2014 Very fast solution to the PnP problem with algebraic outlier rejection *2014 IEEE Conf. on Computer Vision and Pattern Recognition* pp 501–8

Gouveia A R, Metz C, Freire L, Almeida P and Klein S 2017 Registration-by-regression of coronary CTA and X-ray angiography *Comput. Methods Biomech. Biomed. Eng.* **5** 208–20

Groher M, Bender F, Hoffmann R-T and Navab N 2007 Segmentation-driven 2D–3D registration for abdominal catheter interventions *Int. Conf. on Medical Image Computing and Computer-Assisted Intervention* (Berlin: Springer) pp 527–35

Hipwell J H, Penney G P, McLaughlin R A, Rhode K, Summers P, Cox T C, Byrne J V, Noble J A and Hawkes D J 2003 Intensity-based 2D–3D registration of cerebral angiograms *IEEE Trans. Med. Imaging* **22** 1417–26

Jian B and Vemuri B C 2011 Robust point set registration using Gaussian mixture models *IEEE Trans. Pattern Anal. Mach. Intell.* **33** 1633–45

Kang X, Armand M, Otake Y, Yau W-P, Cheung P Y, Hu Y and Taylor R H 2013 Robustness and accuracy of feature-based single image 2d–3d registration without correspondences for image-guided intervention *IEEE Trans. Biomed. Eng.* **61** 149–61

Kerrien E, Berger M-O, Maurincomme E, Launay L, Vaillant R and Picard L 1999 Fully automatic 3D/2D subtracted angiography registration *Int. Conf. on Medical Image Computing and Computer-Assisted Intervention* (Berlin: Springer) pp 664–71

Lepetit V, Moreno-Noguer F and Fua P 2008 EPnP: an accurate O(n) solution to the PnP problem *Int. J. Comput. Vis.* **81** 155

Liu S, Liu P, Li Z, Zhang Y, Li W and Tang X 2017 A 3D/2D registration of the coronary arteries based on tree topology consistency matching *Biomed. Signal Process. Control* **38** 191–9

Markelj P, Tomaževič D, Likar B and Pernuš F 2012 A review of 3D/2D registration methods for image-guided interventions *Med. Image Anal.* **16** 642–61

Miao S, Liao R, Lucas J and Chefd'hotel C 2013 *Augmented Reality Environments for Medical Imaging and Computer-Assisted Interventions* (Berlin: Springer) pp 97–106

Moriconi S, Zuluaga M A, Jäger H R, Nachev P, Ourselin S and Cardoso M J 2018 Elastic registration of geodesic vascular graphs *Int. Conf. on Medical Image Computing and Computer-Assisted Intervention* (Berlin: Springer) pp 810–8

Myronenko A and Song X 2010 Point set registration: coherent point drift *IEEE Trans. Pattern Anal. Mach. Intell.* **32** 2262–75

Nasr-Esfahani E, Karimi N, Jafari M H, Soroushmehr S M R, Samavi S, Nallamothu B and Najarian K 2018 Segmentation of vessels in angiograms using convolutional neural networks *Biomed. Signal Process. Control* **40** 240–51

Pinheiro M A, Kybic J and Fua P 2016 Geometric graph matching using Monte Carlo tree search *IEEE Trans. Pattern Anal. Mach. Intell.* **39** 2171–85

Rivest-Henault D, Sundar H and Cheriet M 2012 Nonrigid 2D/3D registration of coronary artery models with live fluoroscopy for guidance of cardiac interventions *IEEE Trans. Med. Imaging* **31** 1557–72

Segars W P, Sturgeon G, Mendonca S, Grimes J and Tsui B M W 2010 4D XCAT phantom for multimodality imaging research *Med. Phys.* **37** 4902–15

Serradell E, Pinheiro M A, Sznitman R, Kybic J, Moreno-Noguer F and Fua P 2014 Non-rigid graph registration using active testing search *IEEE Trans. Pattern Anal. Mach. Intell.* **37** 625–38

Serradell E, Romero A, Leta R, Gatta C and Moreno-Noguer F 2011 Simultaneous correspondence and non-rigid 3D reconstruction of the coronary tree from single x-ray images *2011 Int. Conf. on Computer Vision* pp 850–7

van de Kraats E B, Penney G P, Tomazevic D, Walsum T V and Niessen W J 2005 Standardized evaluation methodology for 2D–3D registration *IEEE Trans. Med. Imaging* **24** 1177–89

Varnavas A, Carrell T and Penney G 2015 Fully automated 2D–3D registration and verification *Med. Image Anal.* **26** 108–19